Modeling Photon Transport in Fluorescent Solar Concentrators

Thomas S. Parel*, Lefteris Danos[||], Liping Fang and Tomas Markvart

Solar Energy Laboratory, University of Southampton, Southampton, Hampshire, SO17 1BJ, United Kingdom

*Email: T.S.Parel@southampton.ac.uk, Tel: +44 (0) 7514 807 459, Fax: +44 (0) 23 8059 3016

[||] Present address: Department of Chemistry, Lancaster University, Lancaster, LA1 4YB, UK

Abstract — Fluorescent solar concentrators (FSC) can concentrate light onto solar cells by trapping fluorescence through total internal reflection. In an ideal FSC the major obstacle to efficient photon transport is the re-absorption of the fluorescence emitted. In order to decompose the contribution of different photon flux streams within a FSC, the angular dependent re-absorption probability is introduced in this paper and modelled. This is used to analyze the performance of different FSC configurations and is also compared with experimental results. To illustrate the application of the modelling, the collection efficiency of ideal devices has also been calculated from the re-absorption probability and is shown to be useful for estimating non-ideal losses such as those due to scattering or reflection from mirrors. The results also indicate that among the FSCs studied, the performance of those surrounded by four edge solar cells is close to ideal. The rapid optimization of FSCs has also been presented as another practical application of the models presented in this paper.

Keywords — energy, energy conversion, photovoltaic systems, solar energy, solar power generation.

I. Introduction

The main barrier to the widespread utilization of solar energy for electricity generation is higher costs as compared to conventional energy sources. There are a number of approaches to reduce the cost of solar energy [1]. One is to concentrate light in order to reduce the amount of solar cell material required. Concentration of light can be achieved using mirrors and lenses that require direct sunlight or through the use of a fluorescent solar concentrator (FSC) that can also concentrate diffuse light.

A FSC consists of fluorescent molecules embedded within a host material. Solar radiation is absorbed by the fluorescent material and is re-emitted isotropically [2][3]. Emitted photons incident on the top or bottom surface of the FSC at a zenith angle greater than the critical angle, θ_c, will be trapped and concentrated onto the edge [2]-[5]. The thermodynamic efficiency limits for these devices calculated using the detailed balance limit [6][7] indicate the potential to achieve performances close to the Shockley-Queisser limit [8]. In particular, it has been shown that on incorporating a photonic band stop filter to FSCs a theoretical efficiency limit of 26.8% when coupled to silicon solar can be achieved [7].

One technique for modeling the photon transport within FSCs is by calculating the re-absorption probability of certain photon flux streams found within FSCs [4] in order to track the effect of multiple absorption and emission events [9]. The modeling of the re-absorption probability of fluorescence within FSCs began with Weber & Lambe [4] who described a model for the re-absorption probability of the trapped fluorescence within a FSC attached to a single solar cell. The setup they considered is equivalent to a rectangular FSC with a solar cell mounted on one edge and mirrors on the other three edges. This configuration will be referred to by the term 1Cell setup.

In order to maximize edge concentration, re-absorption of trapped fluorescence needs to be avoided. This is because re-absorption can result in either re-emission of photons that escape the FSC through the top or bottom surfaces or loss of the absorbed energy through non-radiative processes. In the 1Cell setup, rays emitted parallel or close to parallel to the solar cell are required to travel a long path length in order to reach the solar cell and therefore their re-absorption probability is large. Furthermore, the reflection from mirrors on edges without a solar cell attached adds additional losses. The use of FSCs with four edge mounted solar cells (4Cell setup) reduces or removes these losses and has therefore been explored extensively [10]. A comparison of the 1Cell and 4Cell setup has been shown in Fig.1.

The highest power conversion efficiencies of FSCs reported in the literature all use the 4Cell setup [11]-[13]. To our knowledge re-absorption models have not been adapted to the 4Cell setup. This paper develops on concepts from [4] and [9] and applies them to the 4Cell setup since this is the most promising configuration for achieving high efficiency FSCs.

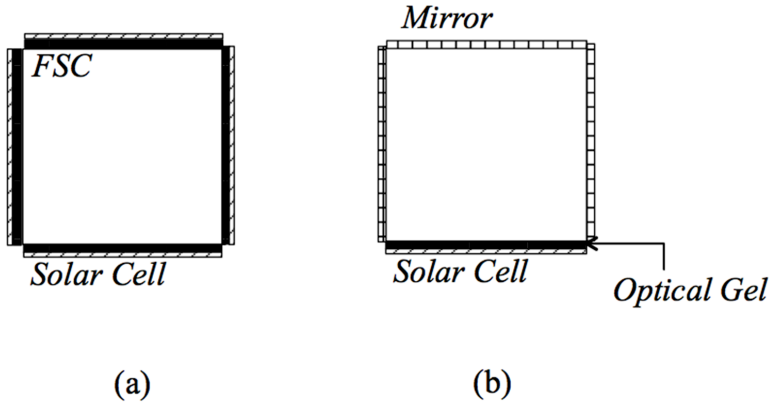

Fig. 1. Comparison of the (a) 4Cell and (b) 1Cell setups. An optical coupling gel is applied on the edge of the solar cell to enable all the light to couple to the solar cell. An air gap is assumed between the mirrors and the collector's edges in order not to disturb the total internal reflection arrangement.

Angular measurements of the photon flux/fluorescence escaping the edge of FSCs have previously been measured in [14][15][16][17] to determine which angles of emission correspond to the greatest loss of photons. A cylindrical lens coupled to the FSC edge in [14] [15] and [16] was used to 'see' inside the FSC. Monte Carlo simulations of the photon flux exiting the FSC edge were also presented in these publications. In [17] the FSC edge was not coupled to a lens and a simple numerical model that qualitatively explains fringe-like patterns detected for spot illumination was presented. However, to our knowledge, angular resolved measurements and modelling of FSCs with edges coupled to solar cells/mirrors has not been

previously reported. Studying photon flux streams of FSCs with edges coupled to solar cells/mirrors is critical since this is how FSCs for photovoltaic applications are used in operation. This paper presents experimental measurements of the angularly resolved photon flux and fluorescence exiting the edge in two of the most common FSC configurations i.e. the 1Cell and 4Cell setups. Models have also been developed to analyze the experimental measurements.

Estimation of non-ideal losses such as due to scattering and reflection losses is shown to be a practical application of the models developed and have been demonstrated for two different methods of fabricating FSCs: i.e. spin coating (Spin-FSC) and molding (Mold-FSC). The utility of these models has further been highlighted by the optimization of the dye concentration of a FSC containing Lumogen F Red 305 dye.

II. THEORY

A FSC of volume V is considered. Assuming uniform illumination over the top surface area of the FSC, the re-absorption probability, r, of the trapped photon flux of wavelength λ in an ideal FSC is given by:

$$1-r(\lambda)=\int\frac{dV}{V}\int_{\Omega_t}\exp\left(-\alpha_{\text{em}}(\lambda)l\right)\frac{d\Omega}{4\pi(1-P)}, \quad (1)$$

where P is the fraction of photons emitted within the escape cones, dV is a small volume element, $d\Omega$ is a small solid angle element, l is a measure of the path length from point of emission to a solar cell and α_{em} is the absorption coefficient at the emission wavelength. Ω_t indicates that the integration is over the solid angle of total internal reflection (i.e. the trapped solid angle). Assuming absorption can be considered to be uniform across the thickness of the FSC and expanding $d\Omega$, we obtain:

$$1-r(\lambda)=\int_0^{2\pi}\frac{d\phi}{2\pi}\int\frac{dA}{A_{top}}\int_{\theta_c}^{\pi-\theta_c}\exp\left(-\alpha_{\text{em}}(\lambda)l\right)\frac{\sin\theta d\theta}{2(1-P)}, \quad (2)$$

where A_{top} is the top surface area of the FSC and dA is a small area element, ϕ and θ are the azimuthal and zenith angles of emission respectively (with θ_c denoting the critical angle for total internal reflection).

The average re-absorption probability of the trapped photon flux, R, is obtained by a weighted average of r over the normalized first fluorescence, f_1 (i.e. re-absorption free fluorescence):

$$R = \int_0^\infty r(\lambda) f_1(\lambda) d\lambda \,. \quad (3)$$

The re-absorption probability for different azimuthal angles of emission, Γ, follows from (2):

$$1 - \Gamma(\phi,\lambda) = \int \frac{dA}{A_{top}} \int_{\theta_c}^{\pi-\theta_c} \exp\left(-\alpha_{em}(\lambda) l\right) \frac{\sin\theta d\theta}{2(1-P)} \,. \quad (4)$$

The average angular re-absorption probability, Γ' is calculated using an expression similar to (3):

$$\Gamma'(\phi) = \int_0^\infty \Gamma(\phi,\lambda) f_1(\lambda) d\lambda \,. \quad (5)$$

Assuming that the wavelength distribution of fluorescence emitted is independent of the excitation wavelength, building upon expressions presented in [9], Γ' can be connected to the average angular collection efficiency in an ideal FSC, ρ i.e. the probability that an absorbed photon results in emission at an angle ϕ that reaches a solar cell:

$$\rho(\phi) = \frac{\phi_f \left\{1 - \Gamma'(\phi)\right\} \frac{(1-P)}{2\pi}}{1 - \phi_f \left[(1-P)R + P\bar{R}\right]}, \quad (6)$$

where $\bar{R}$ is the average re-absorption probability of the escape cone photon flux and ϕ_f is the quantum yield of the fluorescent molecule. The denominator in (6) corresponds to the effect of photon recycling due to re-absorption. From (6) it is clear that $\rho(\phi)$ is directly proportional to 1 - Γ' (ϕ) in an ideal FSC.

The photon flux emitted at an angle ϕ reaching the edge, N_{edge}, can be written as:

$$N_{edge}(\phi) = \rho(\phi) \int Q_a(\lambda) N_{inc}(\lambda) d\lambda \,, \quad (7)$$

where Q_a is the absorption efficiency i.e. fraction of incident photons absorbed by the FSC and N_{inc} is the photon flux incident on the FSC. In (7) the term in the integral is a constant independent of ϕ, therefore:

$$N_{edge}(\phi) \propto \rho(\phi) \propto 1 - \Gamma'(\phi) \,. \quad (8)$$

The above shows that in an ideal FSC, we expect the angular distribution of the photon flux exiting the FSC edge to be proportional to 1 - Γ' (ϕ).

In [18] the collection efficiency, Q_c i.e. the probability that an absorbed excitation photon results in a photon reaching a solar cell, of a FSC is decomposed into an integration over the spectral collection efficiency, χ.
In this paper we can similarly decompose Q_c into an integration over ρ:

$$Q_c = \int_0^{2\pi} \rho(\phi) d\phi. \quad (9)$$

Integrating (9) expressions for Q_c from [9] and [18] are reproduced:

$$\begin{aligned} Q_c &= \frac{\phi_f (1-P)}{1-\phi_f \left[(1-P)R + P\bar{R}\right]} \int_0^{2\pi} \left\{1-\Gamma'(\phi)\right\} \frac{d\phi}{2\pi} \\ &= \frac{\phi_f (1-P)(1-R)}{1-\phi_f \left[(1-P)R + P\bar{R}\right]} \end{aligned} \quad . (10)$$

The optical quantum efficiency (OQE) is the ratio between photons concentrated onto edge mounted solar cells and excitation photons incident on the FSC top surface. In a FSC where the wavelength distribution of fluorescence emitted can be assumed to be independent of the excitation wavelength, the OQE can be written as the product of two terms, a wavelength dependent term related to the absorbance of the FSC and a wavelength independent term i.e. Q_c:

$$OQE(\lambda) = Q_a(\lambda) Q_c. \quad (11)$$

The expressions presented do not include non-ideal losses such as due to scattering or inefficient reflection from mirrors. These non-ideal losses only affect the wavelength independent term, Q_c.

Comparing the difference between ideal models and experimentally measured results would allow the estimation of these non-ideal transport losses in FSCs.

When we consider the 4Cell setup, it is necessary to model the system in two dimensions as can be seen in Fig. 2. ϕ_1 and ϕ_2 in this figure represent the extent of the azimuthal angle of emission from a fluorescent molecule towards the solar cell placed at the edge shown at the top of this figure. The re-absorption probability therefore depends on the solar cell an emitted ray is emitted towards. In a square FSC of length L surrounded by four solar cells (Fig. 2), distance l for a ray emitted towards the top solar cell i.e. as shown in Fig. 2 is given by:

$$l(x,y) = \frac{L-y}{\sin\theta \sin\left(\phi(x,y)\right)}, \quad \phi_1 \le \phi(x,y) < \phi_2. \quad (12)$$

Simple trigonometric arguments that follow from Fig. 2 allows ϕ_1 and ϕ_2 to be determined for emission from a given point in the *xy* plane as well as the two additional azimuthal angles required for a complete description. Dividing a FSC in the 4Cell setup into such distinct position dependent angular regions for calculating the path length has also been used in [19]. That study however focused on the effect of photonic band stop filters coupled to FSCs. Reflection due to the application of such devices to FSCs also depend on the path length of light i.e. there are more reflection events with increasing path length (on average) for emission at a given direction.

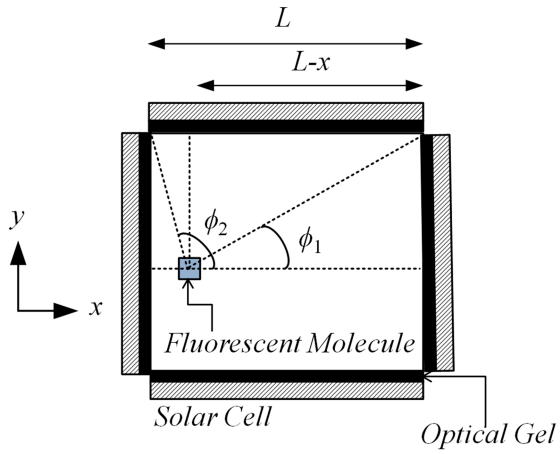

Fig. 2. Top view of the 4Cell setup. The range of azimuthal angles of emission, ϕ_1 and ϕ_2, from a particular fluorescent molecule that can reach the solar cell at the top of this figure has been shown.

Γ and Γ' (and therefore *R*) are obtained from (4) and (5), in addition to (12) for the 4Cell setup and expressions detailed in [4] for the 1Cell setup. From (12) we know that *l* depends on *x* and *y*, from (4) this indicates that Γ (as well as related quantities like *r*, Γ' and R) for the 4Cell setup requires integration over different points in the *xy* plane. The 1Cell setup, however, as explained in [4] can be simplified by an infinite strip (Fig. 3) assuming the edge mirrors orthogonal to the solar cell edge have close to unity reflection. In this case *l* only depends on one axis and therefore the different re-absorption probabilities are calculated by integration over only different points along one axis.

$\overline{R}$ is given by expressions presented in [20] weighted with an absorption distribution with depth (from the Beer Lambert's law). Q_c can then be calculated and used in order to obtain the OQE of an ideal FSC.

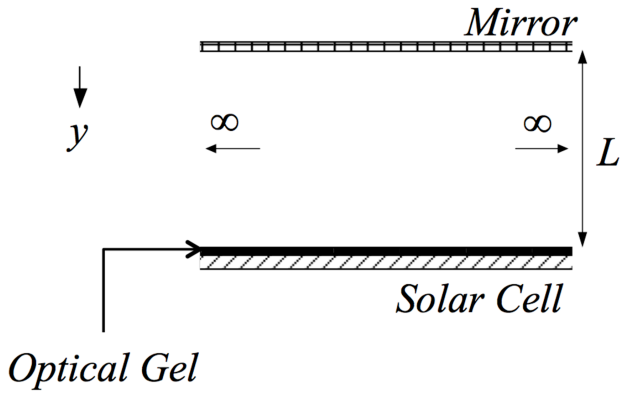

Fig. 3. 1Cell setup simplified by infinite strip. Integration only along one axis is required to calculate *r*.

The OQE can be then connected to the power conversion efficiency of the system η_p, using:

$$\eta_p = \frac{V_{oc} FFq \int N_{inc}(\lambda) OQE(\lambda) EQE \, d\lambda}{\int P_{inc}(\lambda) d\lambda}, \quad (13)$$

where *FF* is the fill factor of the attached solar cells, V_{oc} is the open circuit voltage of the solar cell, *EQE* is the average EQE of the solar cell to incident fluorescence and P_{inc} is the power of the incident light.

III. Experimental

The FSCs used in this study consists of 20 x 20 x 1 mm Mold-FSCs (Teknova AS) and a Spin-FSC consisting of a poly(methyl methacrylate) host material (refractive index equal to 1.49 at 587.6 nm) doped with Lumogen F Red 305 dye (BASF, fluorescent quantum yield equal to 0.95). The Mold-FSCs are doped with dye concentrations of 300 mg/l and 800 mg/l. The Spin-FSC consists of a thin film layer (8 μm thick) doped, in solution, at a concentration of 300 mg/l (in PMMA, Microchem 950 C 10) and deposited onto optical glass (BK7 windows) at 500 rpm (Laurell). The dye-PMMA mixtures were put in a sonicator for 30 minutes and left overnight prior to deposition in order to ensure complete dissolution. The PMMA and glass substrates have a refractive index of 1.52 and reflection loss of 8.1% for 2 surfaces (at 587.6 nm). A glass thickness of 1 mm was selected.

The absorbance of the FSCs was measured using a Bentham spectrometer and an IL1 100 W Halogen light source.

The fluorescence emitted from the FSCs was detected using an Avantes (AvaSpec-2048) spectrometer and an 89 North PhotoFluor II 200 W Metal Halide lamp (excitation at 440 nm). The first fluorescence was obtained for the Mold-FSCs by grinding down and measuring the top fluorescence. For the Spin-FSC, the top fluorescence of a low dye concentration sample was used to obtain the first fluorescence.

A solar simulator (T.S. Space Systems) equipped with a 300 W Xenon lamp approximating

the AM1.5 spectrum and a filter selection wheel (350−1100 nm, step 50 nm) was used to measure the current output of the solar cell(s) coupled to the FSCs. The Xenon lamp was calibrated using a silicon standard solar cell calibrated at the National Renewable Energy Laboratory (NREL) for standard test conditions (AM 1.5, 1000 W/m^2 at 25°C).

Optical gel (Thorlabs) was used for index matching (refractive index of 1.46 at 589.3 nm) between the solar cell and the FSC. Index matching gel applied at the interface between the FSC and the solar cell ensures that light from a full hemisphere reaches the solar cell.

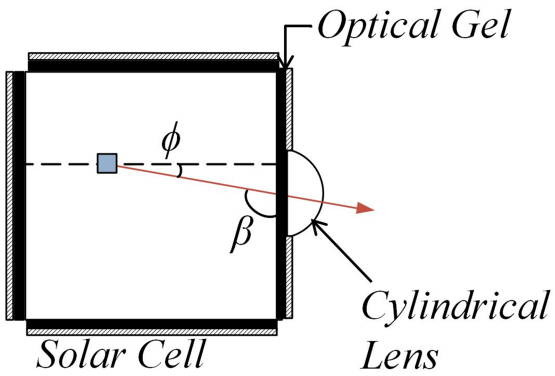

Fig. 4. Angles ϕ and β in the 4Cell setup. It is clear that measurements made at an angle β with respect to a particular solar cell can be related to emission at a specific angle ϕ.

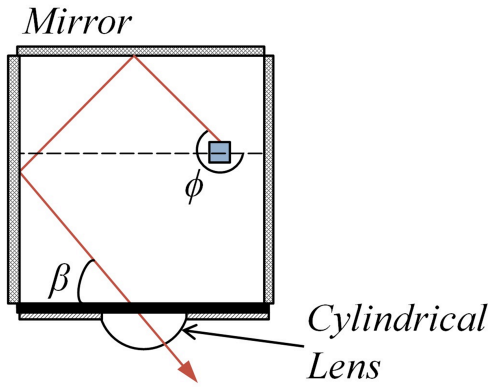

Fig. 5. Angles ϕ and β in the 1Cell setup. For the 1Cell setup measurements made at a given angle β is the effect of emission at two different azimuthal angles of emission ϕ i.e. emission towards the solar cell and emission reflected by the mirror opposite to the solar cell.

The emission was analyzed as a function of angle from the edge of the FSC by attaching a square silicon photo diode (Thorlabs, 1 mm x 1 mm) to a motorised system. The detector was setup to move in a semi-circle at a distance of 8 cm about the central point of the FSC edge, within in a plane parallel to the FSC top surface (Fig. 4 and Fig. 5 shows the plane of rotation). The emission spectrum of the edge emission was also analyzed as a function of the emission angle and an iris diaphragm was attached at the detector to limit the angular range detected. A flexible silicon solar cell (Sol Expert Group) was used to measure the photon flux

reaching a 1 mm thick semi-circle 8 cm from the FSC edge and used to normalize the area under the angular distribution. The FSC was illuminated uniformly at the top surface by a LED Luxeon light source.

A single 15 mm focal length lens was attached at the edge of the FSC in order to directly lead the detected light towards the detector without refraction or reflection affecting its path. Optical gel was also used to couple the FSC edge to the lens. Finally, a thin black surface was used as a blind in order to block any light coming from directions other than the FSC edge from reaching the detector.

IV. Results and Discussion

a. Photon Flux and Fluorescence with Angle

A study of the angular characteristics of the fluorescence exiting the FSC edge has been conducted for different azimuthal angles of emission (the setup is as shown in Fig. 4 and Fig. 5).

The models described have been used to study the photon transport for the 1Cell and 4Cell setups. For simplicity, photon transport at only the peak emission wavelength, i.e. 600 nm (absorption coefficient equal to 0.8 mm^{-1}) will be described. Γ calculated using the analytical models of the two setups is shown in Fig. 6 for fixed dimensions of the FSC while in Fig. 7 the gain is fixed (the gain is defined as the ratio between the FSC top surface area and edge solar cell area).

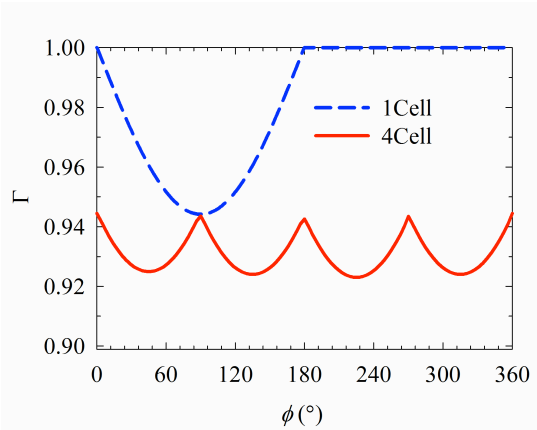

Fig. 6. The angular dependence of the re-absorption probability shown for the 4Cell and 1Cell setups for fixed FSC dimensions (theory).

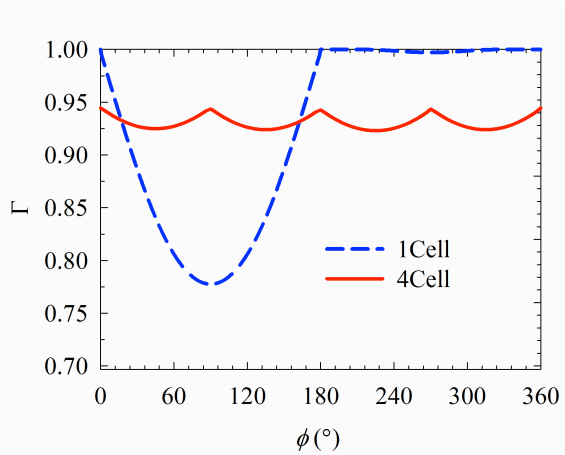

Fig. 7. The angular dependence of the re-absorption probability shown for the 4Cell and 1Cell setups for a fixed FSC gain (theory).

The results indicate that the variation of Γ with ϕ for the 4Cell setup is fairly constant. For the 1Cell setup, Γ is seen to go to unity for azimuthal angles of emission close to parallel to the edge coupled to a solar cell due to long path lengths.

Furthermore, there is a significant difference in Γ for fluorescence emitted towards and away from the solar cell. Though the calculated Γ is large for the sample and setups considered, due to the high quantum yield of the fluorescent species re-absorption results in photon recycling. Most of the photons are, therefore, eventually emitted from the FSC and the re-absorption probability affects only the ratio of how many leave through the entrance aperture or hit a solar cell.

For the 4Cell setup it is noticed that photons emitted at an azimuthal angle normal to a particular solar cell surface (i.e. ϕ close to 0°, 90°, 180°, 270°) have a higher re-absorption probability. This is likely because rays emitted at these angles, irrespective of the distance between the point of emission and the relevant solar cell, can only reach one particular solar cell and therefore travel longer path lengths on average. It is noticed that when the dimensions of the FSC are kept constant the fluorescence within the 4Cell setup experiences significantly lower re-absorption while when the gain is fixed the total re-absorption (as represented by the area under the curves) is similar for both setups. This indicates that in ideal FSCs, the performance should be similar for both configurations if the gain is kept constant. These results also indicate that though re-absorption increases with increasing A_{top}, adjusting the gain accordingling i.e. by also increasing the FSC thickness, the performance of FSCs can be maintained (Q_{a} must also be maintained by adjusting the dye concentration).

Fig. 8 shows the experimentally measured variation in the photon flux of emission reaching the edge(s) for the 4Cell and 1Cell setups (fixed FSC dimensions) with the azimuthal angle of incidence on the solar cell (β). The plotted curves have been normalized such that the integration over all angles gives the photon flux measured by the flexible solar (note that the total photon flux for the 4Cell setup is four times the photon flux measured by the flexible solar cell at one edge).

The angle β is as shown in Fig. 4 and Fig. 5. For both configurations it is clear that the photon flux decreases for angles close to parallel to a given edge mounted solar cell. Furthermore, as expected (due to lower re-absorption) more photons reach the edge(s) in the 4Cell than in the 1Cell setup.

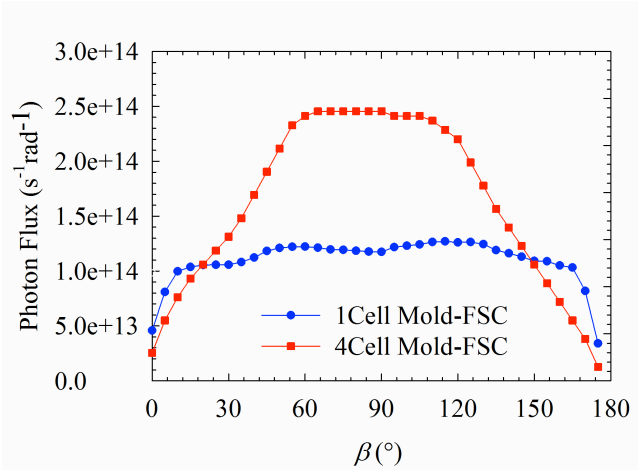

Fig. 8. The photon flux reaching a solar cell in the 1Cell and 4Cell Mold-FSCs with angle β.

Spectroscopic measurements strongly indicate that the reduction in photon flux at certain angles for the two different configurations is for very different reasons. For the 4Cell setup it is in fact seen that fluorescence reaching the FSC edge at azimuthal angles close to parallel to the edge (i.e. ϕ close to 0°) is blue-shifted compared to fluorescence incident perpendicular to the edge (Fig. 9). This indicates that re-absorption is lower at angles close to parallel to the solar cell. This could be because for emission at steep angles to reach a given solar cell, the point of emission must be very close to the FSC edge otherwise this emission will reach another solar cell. This also explains why the distribution of the photon flux with angle β is only large for a smaller range of angles for the 4Cell setup. The situation is seen to be reversed for the 1Cell setup where the spectra indicates that the re-absorption probability increases from emission perpendicular to parallel to the edge mounted solar cell as seen by the corresponding red-shift (Fig. 10).

In [18] it is described how r can be obtained from experimental measurements of the fluorescence distribution of a photon flux stream i.e. by fitting the measured spectrum with the f_1 spectrum at long wavelengths where low re-absorption is expected and comparing the relative decrease at short wavelengths. In order to estimate the fluorescence distribution likely to be 'seen' by the solar cell in the 1Cell and 4Cell setups, the reverse of this technique has been used i.e. from the theoretical calculations of r from (2), f_1 has been scaled so as to obtain the fluorescence spectrum expected to reach the solar cell. The results are shown in Fig. 11. As expected, for the 1Cell setup the spectrum reaching the solar cell should be red shifted with respect that of the 4Cell setup (fixed FSC dimensions).

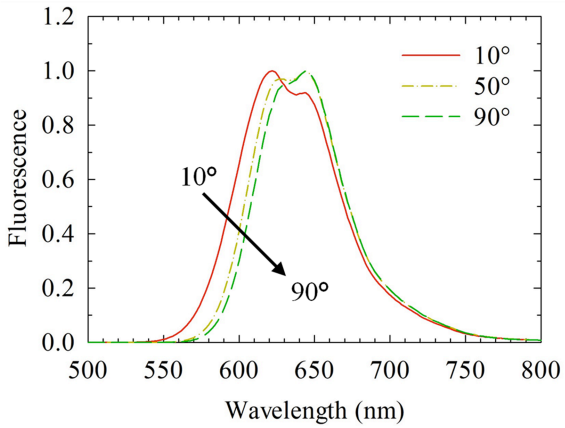

Fig. 9. Spectra of emission reaching the solar cell between 10° and 90° in the 4Cell Mold-FSC.

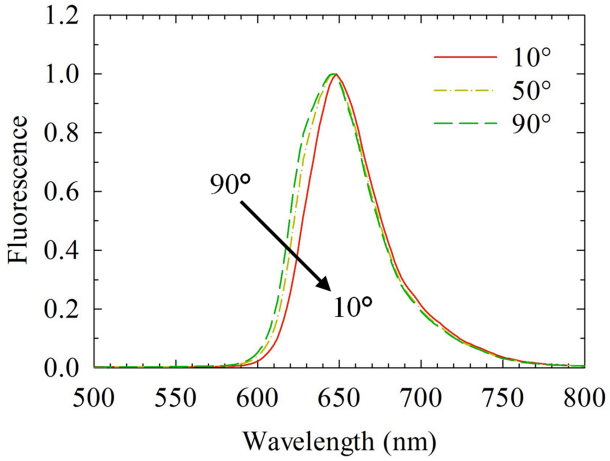

Fig. 10. Spectra of emission reaching the solar cell between 10° and 90° in the 1Cell Mold-FSC.

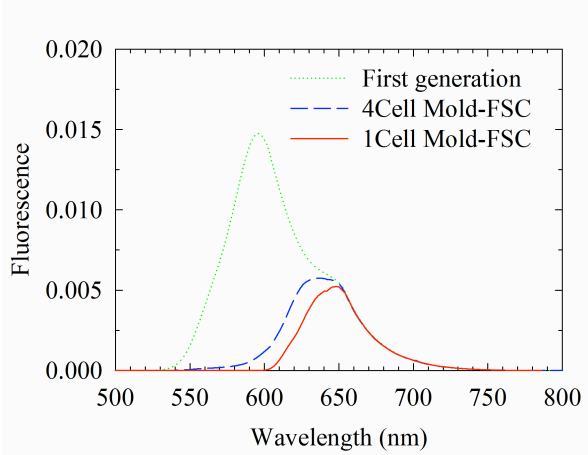

Fig. 11. Spectra of total emission reaching the solar cell in the 1Cell and 4Cell Mold-FSCs calculated from r and the measured first generation fluorescence, f_1. f_1 has been normalized so as to represent a probability distribution.

Assuming that in the 4Cell setup each solar cell sees the same distribution of the photon flux with angle β, then a summation of these photon fluxes will give the photon flux distribution according to emission angle ϕ reaching a solar cell. To compare this with the modelling, Γ' has been calculated from Γ using (5) for the 300 mg/l Mold-FSC. The results have been plotted in Fig. 12. It is seen that the angular distribution of the photon flux shows the same pattern as the calculated angular distribution of 1 - Γ'. This is consistent with (8) i.e. the photon flux exiting the edge of an ideal FSC is directly proportional to 1 - Γ' (ϕ). The angular results are, therefore, consistent with the performance of the 4Cell Mold-FSC being well described by ideal models.

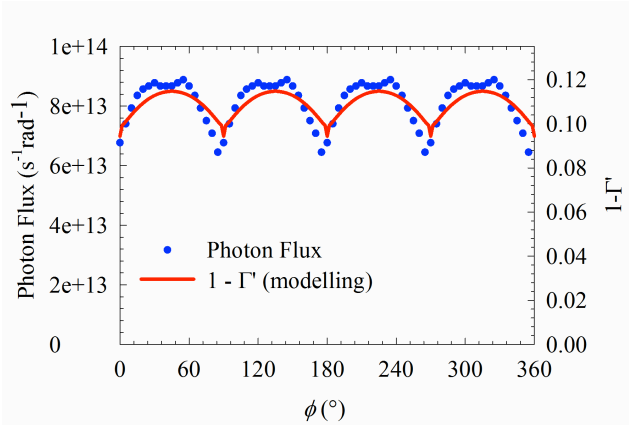

Fig. 12. The photon flux reaching a solar cell in the 4Cell Mold-FSC with angle ϕ compared with 1 - Γ'.

b. Optical Quantum efficiency and Non-Ideal Losses

Comparisons between calculated and experimental OQE for 4Cell Mold-FSCs are shown in Fig. 13 and Fig. 14 and shows good agreement. This again indicates that the losses of these devices are described well by the ideal model.

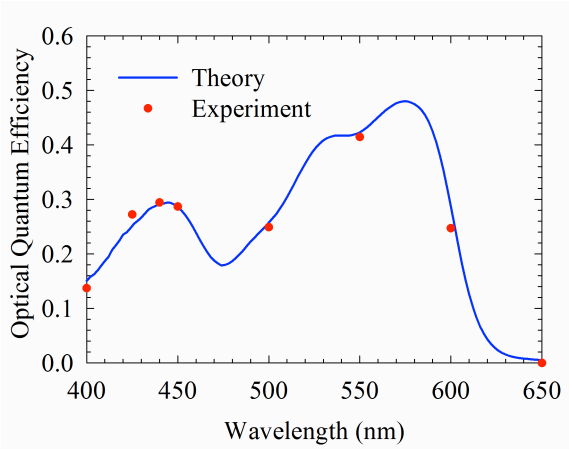

Fig. 13. Theoretical and experimental OQE of a 4Cell Mold-FSC doped at 300 mg/l.

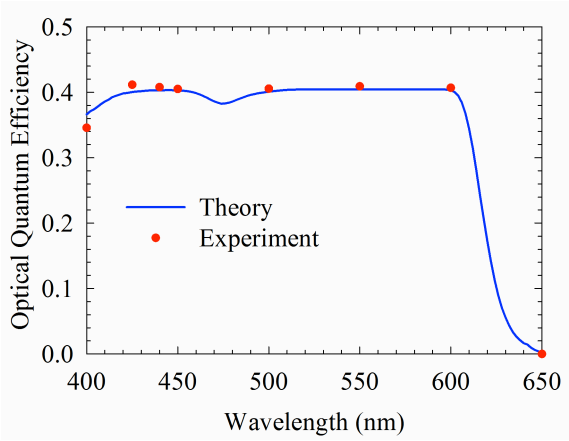

Fig. 14. Theoretical and experimental OQE of a 4Cell Mold-FSC doped at 800 mg/l.

On comparing the calculated OQE with experimental results of a Mold-FSC and Spin-FSC (both doped at 300 mg/l) in the 1Cell setup (Fig. 15 and Fig. 16), the presence of non-ideal losses is apparent. For the Mold-FSC in the 1Cell setup we notice a 22% drop in the OQE across all absorbing wavelengths. This wavelength independent difference indicates that this is due to non-ideal transport losses most likely due to reflection at edges coupled to mirrors. For the Spin-FSC this loss increases to 75%. Since the Spin-FSC lacks uniformity especially at the edges, one possible cause for the large increase in loss compared to the Mold-FSC could be due to scattering in the thin film layers. Indeed, a previous study of a similarly fabricated Spin-FSC (un-doped) indicated that scattering due to surface roughness accurately described measurements of the light propagation at different angles in the device [21].The ability to quantify these non-ideal losses would be useful in the optimization and design of non-ideal FSCs.

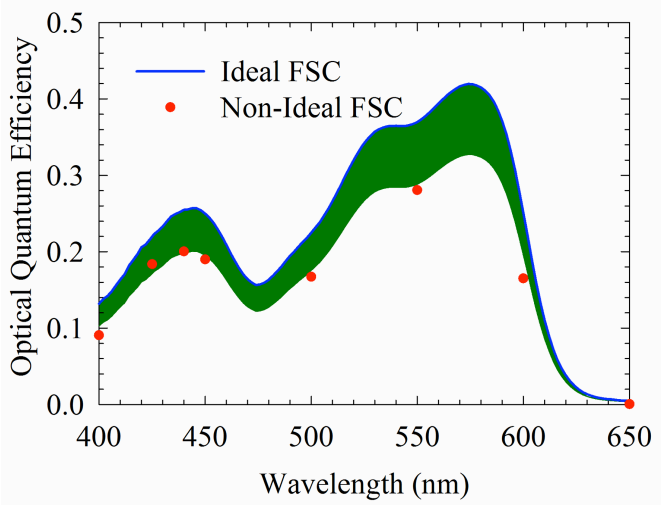

Fig. 15 Theoretical and experimental OQE of a 1Cell Mold-FSC. Scaling the theoretical results down by 22% fits the experimental measurements. This scaling factor is likely due to non-ideal transport losses.

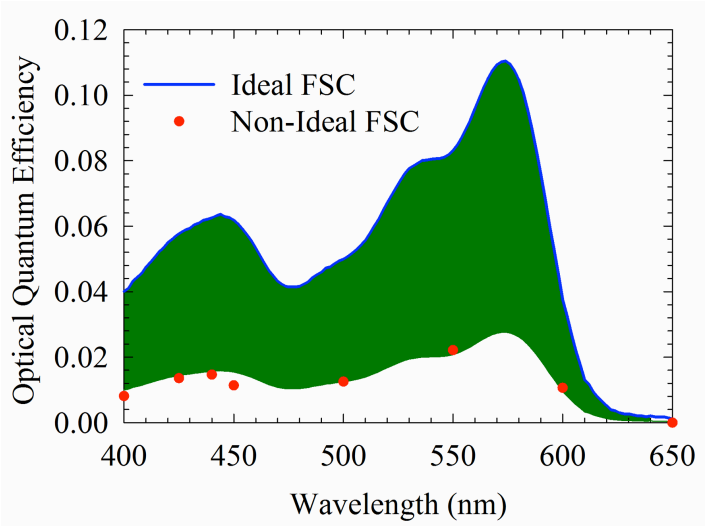

Fig. 16. Theoretical and experimental OQE of a 1Cell Spin-FSC. Scaling the theoretical results down by 75% fits the experimental measurements. This scaling factor is likely due to non-ideal transport losses.

c. Optimization of FSCs

The dye concentrations of FSCs doped with Lumogen F Red 305 dye has been optimized using the models developed for the 4Cell setup to illustrate their predictive ability for a practical FSC. The OQE has been calculated for different dye concentrations for Mold-FSCs as shown in Fig. 17. The FSCs modelled contain dye concentrations of integer multiples of the 300 mg/l FSC fabricated and characterized. It is seen that as the dye concentrations increase, the OQE become flatter across absorbing wavelengths. A peak OQE close to 50% for excitation at 570 nm is seen on doubling the dye concentration of the 300 mg/l doped Mold-FSC.

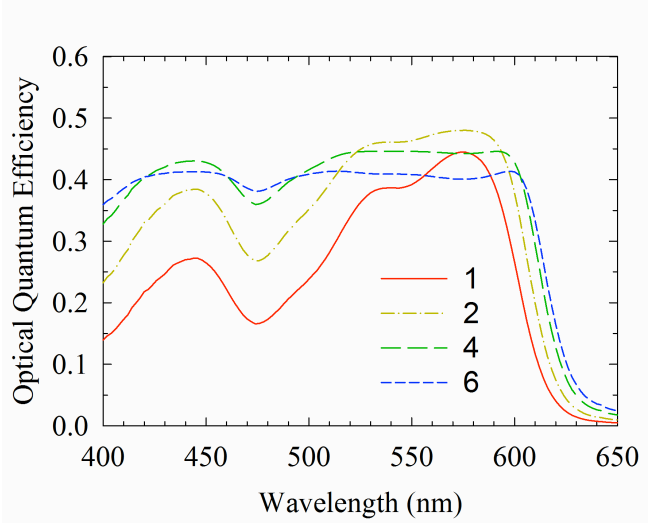

Fig. 17. OQE for increasing dye concentrations. The numbers in the legend indicate the dye concentrations of Mold-FSCs relative to the 300 mg/l sample. The results show the effect of dye concentration on the OQE.

On increasing the dye concentration further a decrease in the peak OQE is seen due to the competing requirements for high Q_a and Q_c. After a certain dye concentration the benefit of greater absorption does not compensate for the higher re-absorption resulting in a decrease in the Q_c (as indicated by (6), (9) and (11)).

Fig. 18 shows the power conversion efficiency calculated from (13) when coupled to four gallium arsenide solar cells. The solar cells are assumed to have an open circuit voltage equal to 1.11 and a fill factor or 0.87 [22] (it is assumed that the increase in open circuit voltage with concentration is negligible). The fluorescence incident on the solar cell is also assumed to be converted with an EQE of 0.95.

The results indicate a power conversion efficiency of close to 3% can be obtained for the 300 mg/l doped Mold-FSC. The highest power conversion efficiency that can be obtained for a FSC based on Lumogen Red F 305 dye (for the given FSC dimensions) is close to 4.5% and requires the dye concentration four times that of the Mold-FSC doped at 300 mg/l. For even larger dye concentrations a slight decrease in power conversion efficiency is expected due to the effect of re-absorption. The optimisation results shown in Fig. 18 are consistent with efficiency measurements previously reported i.e. 3.3% in [23] and 2.4% in [24], for FSCs consisting of only Lumogen Red dye. Both of these studies were carried out, however, for the 1Cell setup and used crystalline silicon solar cells. The FSCs used also had a much larger gain. These factors are all expected and seen to result in lower power conversion efficiencies compared to the maximum of the optimization results presented in Fig.18.

Two approaches are required for FSCs to achieve higher power conversion efficiencies. Firstly, the FSC needs to absorb light over a wider range of wavelengths. This involves the use of multiple fluorescent species. Secondly the negative effects of re-absorption must be reduced. Indeed, the effect of re-absorption is clear in the OQE results shown in Fig. 14. The OQE of the 4Cell Mold-FSC doped at 800 mg/l is flat from 400 nm to 600 nm unlike the OQE for the 300 mg/l doped FSC in the same configuration. (i.e. Fig. 13). This indicates that the wavelength dependent term Q_a from (11) is a constant. Indeed, the absorbance of the 800 mg/l doped FSC is so large that nearly all the light is absorbed in this wavelength range. If there was no re-absorption, the only loss would be due to the escape cones (close to 25% for a PMMA based FSC) and since the quantum yield of the fluorescent species is high an OQE of close to 0.75 between 400 nm to 600 nm would be expected. Due to the effects of re-absorption, the OQE is seen to decrease to 0.40. Clearly the effect of re-absorption is large.

The use of multiple fluorescent species with strong non-radiative energy transfer could be one strategy for decreasing the re-absorption loss [12]. Novel methods such as the use of photonic crystals doped with fluorescent molecules also represent an alternative method for achieving lower re-absorption in FSCs [25].

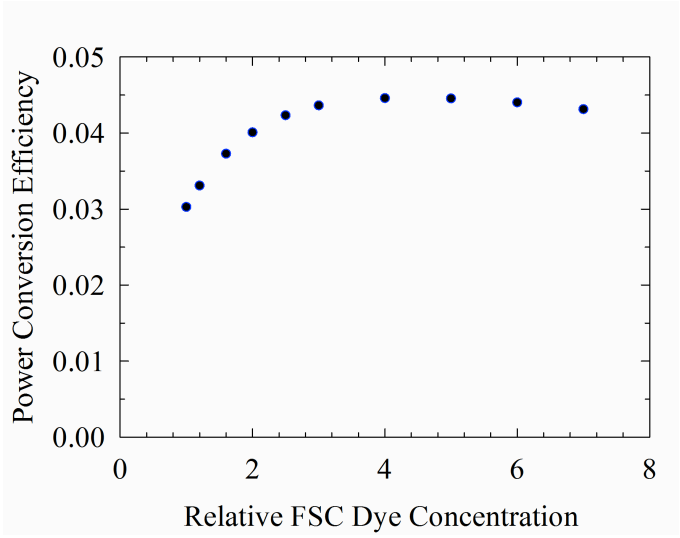

Fig. 18. Power conversion efficiency for increasing dye concentrations. The numbers on the x-axis indicate the dye concentrations of Mold-FSCs relative to the 300 mg/l sample. In this manner the dye concentration for an FSC containing Lumogen Red F 305 dye has been optimized for maximum power conversion efficiency.

V. Conclusion

A model describing the re-absorption probability of the trapped photon flux in FSCs coupled to four edge mounted solar cells has been developed. It has been used to show that the 4Cell setup is fundamentally different to the 1Cell setup in terms of its re-absorption characteristics as a function of the azimuthal angle of emission. However, it is seen that if the gain of the FSC is kept constant both setups should result in similar levels of total re-absorption in ideal FSCs. The performance of the Mold-FSCs in 4Cell setup is seen to be close to ideal as indicated by the angular resolved results which show that the experimentally measured photon flux is directly proportional to calculations of $1 - \Gamma'(\phi)$, which is consistent with what is expected for an ideal FSC.

Calculations of the OQE from re-absorption models compared with experimental measurements also show that the 4Cell Mold-FSCs studied are well described by ideal models. Practical applications of the models developed are shown to include estimation of non-ideal losses and optimisation of power conversion efficiencies.

Acknowledgement

This work has benefitted from the Sustainable Power Generation and Supply, Photovoltaics for the 21st Century (SuperGen PV21) Initiative and the Engineering and Physical Sciences Research Council (EPSRC). We would also like to thank Teknova AS for supplying the molded fluorescent solar concentrators.

REFERENCES

[1] Luque A and Hegedus S. *Handbook of Photovoltaic Science and Engineering*. Wiley: Chichester, 2003. DOI: 10.1002/0470014008.

[2] Shurcliff WA and Jones RC. The trapping of fluorescent light produced within objects of high geometrical symmetry. *Journal of the Optical Society of America* 1949; **39**: 912-916. DOI: 10.1364/JOSA.39.000912.

[3] Garwin RL. The collection of light from scintillation counters. *Review of Scientific Instruments* 1960; **31**: 1010-1011. DOI: 10.1063/1.1717105.

[4] Weber WH and Lambe J. Luminescent greenhouse collector for solar radiation. *Applied Optics* 1976; **15**: 2299-2300. DOI: 10.1364/AO.15.002299.

[5] Goetzberger A and Greubel W. Solar energy conversion with fluorescent collectors. *Applied Physics* 1977; **14**: 123-129. DOI: 10.1007/BF00883080.

[6] Rau U, Einsele F and Glaeser GC. Efficiency limits of photovoltaic fluorescent collectors. *Applied Physics Letters* 2005; **87**: 171101 1-3. DOI: 10.1063/1.2112196.

[7] Markvart T. Detailed balance method for ideal single-stage fluorescent collectors. *Journal of Applied Physics* 2006; **99**: 026101 1-3. DOI: 10.1063/1.2160710.

[8] Shockley H and Queisser W. Detailed balance limit of efficiency of p-n junction solar cells. *Journal of Applied Physics* 1961; **32**: 510-519. DOI: 10.1063/1.1736034.

[9] Batchelder JS, Zewail AH and Cole T. Luminescent solar concentrators. 1: theory of operation and techniques for performance evaluation. *Journal of Applied Optics* 1979; **20**: 3733-3110. DOI: 10.1364/AO.18.003090.

[10] Zastrow A. *Physikalische analyse der energieverlustmechanismen in fluorescenkollector*. Albert-Ludwigs-Universität: Frieburg, 1981.

[11] Sloof LH, Bende EE, Burgers AR, Budel T, Pravettoni M, Kenny RP, Dunlop ED and Büchtemann A. A luminescent solar concentrator with 7.1% efficiency. *Physica Status Solidi- Rapid Research Letters* 2011; **2**: 257-259. DOI: 10.1002/pssr.200802186.

[12] Currie MJ, Mapel JK, Heidel TD, Goffri S and Baldo MA. High-efficiency organic solar concentrators for photovoltaics. *Science* 2008; **321**: 226-228. DOI: 10.1126/science.1158342.

[13] Goldschmidt JC, Peters M, Bösch A, Helmers H, Dimroth F, Glunz SW and Willeke G. Increasing the efficiency of fluorescent concentrator systems. *Solar Energy Materials and Solar Cells* 2008; **93**: 176–182. DOI: 10.1016/j.solmat.2008.09.048.

[14] Goldschmidt JC, Peters M, Prönneke L, Steidl L, Zentel R, Bläsi B, Gombert A, Glunz S, Willeke G and Rau U. Theoretical and Experimental Analysis of Photonic Structures for

Fluorescent Concentrators with Increased Efficiencies. *Physica Status Solidi A* 2008; **205**: 2811-2821. DOI: 10.1002/pssa.200880456.

[15] Bendig M, Hanika J, Peters M, Dammertz H, Weber M and Goldschmidt JC. Simulation of Fluorescent Concentrators. *IEEE/EG Symposium on Interactive Ray Tracing* 2008; Los Angeles, USA. DOI: 10.1109/RT.2008.4634628.

[16] Goldschmidt JC. *Novel Solar Cell Concepts*. Verlay Dr. Hut: München, 2009.

[17] Sträter H, Knabe S, Meyer TJJ and Bauer G. Spectrally and Angle-Resolved Emission of Thin Flm Fuorescence Collectors. *Progress in Photovoltaics: Research and Applications* 2011; **21**: 554-560. DOI: 10.1002/pip.1228.

[18] Kittidachachan P, Danos L, Meyer TJJ, Alderman N and Markvart T. Photon Collection Efficiency of Fluorescent Solar Collectors. *Chimia* 2007; **61**: 780-786. DOI: 10.2533/chimia.2007.780.

[19] Peters M, Goldschmidt JC, Löper P, Bläsi B and Gombert A. The effect of photonic structures on the light guiding efficiency of fluorescent concentrators. *Journal of Applied Physics* 2009; **105**: 014909 1-10. DOI: 10.1063/1.2996081.

[20] Fang L, Parel T, Danos L, and Markvart T. Photon reabsorption in fluorescent solar collectors. *Journal of Applied Physics* 2012; **111**: 076104-076104-3. DOI: 10.1063/1.3702815.

[21] Soleimani N, Knabe S, Bauer GH, Markvart T and Muskens OL. Role of light scattering in the performance of fluorescent solar collectors. *Journal of Photonics for Energy* 2012; **2**: 021801 1-10. DOI: 10.1117/1.JPE.2.021801.

[22] Green MA, Emery K, Hishikawa Y, Warta W and Dunlop ED. Solar Cell Efficiencies Tables (version 39). *Progress in Photovoltaics: Research and Applications* 2011. **20**: 12-20. DOI: 10.1002/pip.2163.

[23] Gallagher SJ, Norton B and Eames PC. Quantum dot solar concentrators: Electrical conversion efficiencies and comparative concentrating factors of fabricated devices. *Solar Energy* 2007; **81**: 813-821. DOI: 10.1016/j.solener.2006.09.011.

[24] van Sark WGJHM, Barnham KWJ, Slooff, LH, Chatten AJ, Büchtemann A, Meyer A, McCormack SJ, Koole R, Farrell DJ, Bose R, Bende EE, Burgers AR, Budel T, Quilitz J, Kennedy M, Meyer T, De Mello Donegá C, Meijerink A and Vanmaekelbergh D. Luminescent solar concentrators: a review of recent results. *Optics Express* 2008; **16**: 21773-21792. DOI: 10.1364/OE.16.021773.

[25] Goldschmidt JC, Peters M, Gutmann J, Steidl L, Zentel R, Bläsi B and Hermle, M. Increasing Fluorescent Concentrator Light Collection Efficiency by Restricting the Angular Emission Characteristic of the Incorporated Luminescent Material: the 'Nano-Fluko' Concept. *Proceedings of SPIE Photonics for Solar Energy Systems III* 2010; Brussels, Belgium. 77250S 1-11. DOI: 10.1117/12.854278.